Higgs and supersymmetry

Journal Article

Author(s):
Buchmueller, Oliver; Cavanaugh, Richard; De Roeck, Albert; Dolan, Matthew J.; Ellis, Jonathan R.; Flächer, Henning; Heinemeyer, Sven; Isidori, Gino; Marrouche, Jad; Martínez Santos, Diego; Olive, Keith A.; Rogerson, S.; Ronga, Frédéric J.; De Vries, K.J.; Weiglein, Georg

Publication date:
2012-06

Permanent link:
https://doi.org/10.3929/ethz-b-000052504

Originally published in:
The European Physical Journal C 72(6), https://doi.org/10.1140/epjc/s10052-012-2020-3

Eur. Phys. J. C (2012) 72:2020
DOI 10.1140/epjc/s10052-012-2020-3

THE EUROPEAN PHYSICAL JOURNAL C

Regular Article - Theoretical Physics

Higgs and supersymmetry

O. Buchmueller[1], R. Cavanaugh[2,3], A. De Roeck[4,5], M.J. Dolan[6], J.R. Ellis[7,4], H. Flächer[8], S. Heinemeyer[9], G. Isidori[10], J. Marrouche[1], D. Martínez Santos[4], K.A. Olive[11,a], S. Rogerson[1], F.J. Ronga[12], K.J. de Vries[1], G. Weiglein[13]

[1]High Energy Physics Group, Blackett Laboratory, Imperial College, Prince Consort Road, London SW7 2AZ, UK
[2]Fermi National Accelerator Laboratory, P.O. Box 500, Batavia, IL 60510, USA
[3]Physics Department, University of Illinois at Chicago, Chicago, IL 60607-7059, USA
[4]CERN, 1211 Genève 23, Switzerland
[5]Antwerp University, 2610 Wilrijk, Belgium
[6]Institute for Particle Physics Phenomenology, University of Durham, South Road, Durham DH1 3LE, UK
[7]Theoretical Particle Physics and Cosmology Group, Department of Physics, King's College London, London WC2R 2LS, UK
[8]H.H. Wills Physics Laboratory, University of Bristol, Tyndall Avenue, Bristol BS8 1TL, UK
[9]Instituto de Física de Cantabria (CSIC-UC), 39005 Santander, Spain
[10]INFN, Laboratori Nazionali di Frascati, Via E. Fermi 40, 00044 Frascati, Italy
[11]William I. Fine Theoretical Physics Institute, School of Physics and Astronomy, University of Minnesota, Minneapolis, MN 55455, USA
[12]Institute for Particle Physics, ETH Zürich, 8093 Zürich, Switzerland
[13]DESY, Notkestrasse 85, 22607 Hamburg, Germany

Received: 3 January 2012 / Revised: 9 February 2012 / Published online: 7 June 2012

Abstract Global frequentist fits to the CMSSM and NUHM1 using the `MasterCode` framework predicted $M_h \simeq 119$ GeV in fits incorporating the $(g-2)_\mu$ constraint and $\simeq$126 GeV without it. Recent results by ATLAS and CMS could be compatible with a Standard Model-like Higgs boson around $M_h \simeq 125$ GeV. We use the previous `MasterCode` analysis to calculate the likelihood for a measurement of any nominal Higgs mass within the range of 115 to 130 GeV. Assuming a Higgs mass measurement at $M_h \simeq 125$ GeV, we display updated global likelihood contours in the $(m_0, m_{1/2})$ and other parameter planes of the CMSSM and NUHM1, and present updated likelihood functions for $m_{\tilde{g}}, m_{\tilde{q}_R}$, BR$(B_s \to \mu^+\mu^-)$ and the spin-independent dark matter cross section $\sigma_p^{\rm SI}$. The implications of dropping $(g-2)_\mu$ from the fits are also discussed. We furthermore comment on a hypothetical measurement of $M_h \simeq 119$ GeV.

1 Introduction

Taking into account the relevant experimental constraints, the CMSSM and NUHM1 predict that the lightest Higgs boson should have couplings similar to those of the Standard Model (SM) Higgs boson [1–3], and that it should weigh no more than ∼130 GeV [4–18]. We recently reported the results of global frequentist fits within the CMSSM and NUHM1 to the first ∼1/fb of LHC data, also including precision electroweak and flavor measurements and the XENON100 upper limit on elastic spin-independent dark matter scattering [3], updating the results of previous global fits by ourselves [19–26] and others[1,2] [27–45] (see also [46]). The results reported in [3] included likelihood contours in the $(m_0, m_{1/2})$, $(\tan\beta, m_{1/2})$ and $(M_A, \tan\beta)$ planes of the CMSSM and NUHM1, as well as $\Delta\chi^2$ functions for $m_{\tilde{g}}$, BR$(B_s \to \mu^+\mu^-)$, M_h, M_A and sparticle production thresholds in e^+e^- annihilation.

Notable predictions of these global fits included $M_h = 119.1^{+3.4}_{-2.9}$ GeV in the CMSSM and $M_h = 118.8^{+2.7}_{-1.1}$ GeV in the NUHM1 (which should be combined with an estimated theory error $\Delta M_h = \pm 1.5$ GeV). These two fits are based solely on the Higgs-*independent* searches including the $(g-2)_\mu$ constraint, i.e., they do not rely on the existing limits from LEP [47, 48], the Tevatron [49], or the LHC [50, 51]. These predictions increase to $M_h = 124.8^{+3.4}_{-10.5}$ GeV in the CMSSM and $126.6^{+0.7}_{-1.9}$ GeV in the NUHM1 if the $(g-2)_\mu$ constraint is dropped.

Subsequently, the ATLAS and CMS Collaborations have released their official combination of the searches for

[a] e-mail: olive@physics.umn.edu

[1]For a sampling of other pre-LHC analyses, see [27–33].

[2]For a sampling of other post-LHC analyses, see [34–45].

a SM Higgs boson with the first ∼1/fb of LHC luminosity at $E_{\rm cm} = 7$ TeV [52–54]. Impressively, the combination excludes a SM Higgs boson with a mass between 141 and 476 GeV. Most recently, the ATLAS and CMS Collaborations have presented preliminary updates of their results with ∼5/fb of data [55]. These results may be compatible with a SM-like Higgs boson around $M_h \simeq 125$ GeV, though CMS also report an excess at $M_h \simeq 119$ GeV in the ZZ^* channel. We recall that, for low values of M_h, the SM electroweak vacuum would be unstable [56], decaying into a state with Higgs vev $>10^8$ (10^{10}) GeV if $M_h = 119(125)$ GeV, and that a very plausible mechanism for stabilizing the vacuum is supersymmetry (SUSY) [57].

In this paper, we first report the likelihood function for an LHC measurement of M_h with a nominal value $\in (115, 130)$ GeV, incorporating the theoretical error ± 1.5 GeV and an estimate ± 1 GeV of the possible experimental error. In both the CMSSM and NUHM1, this likelihood function is minimized for $M_h \simeq 119$ GeV if $(g-2)_\mu$ is included, and is contained within the theoretical uncertainty range shown previously as a 'red band' [3]. We then discuss the consequences of combining a measurement of $M_h \simeq 125$ GeV (assuming that the current excess will be confirmed with more integrated luminosity) with our previous analysis [3] of constraints on the CMSSM and NUHM1 including $(g-2)_\mu$.

We find that the best-fit values of m_0 and $m_{1/2}$ in the CMSSM and NUHM1 are moved to substantially higher values, especially in the case of $m_{1/2}$. We also update our results on the best-fit regions in the $(m_{1/2}, \tan\beta)$ and $(M_A, \tan\beta)$ planes, where we find again the substantial increase in $m_{1/2}$, as compared with our pre-LHC M_h results. We present the corresponding one-dimensional likelihood functions for the gluino mass $m_{\tilde g}$, an average right-handed squark mass $m_{\tilde q_R}$, the lighter scalar tau mass, $m_{\tilde\tau_1}$, as well as in the $(m_{\tilde\chi_1^0}, \sigma_p^{\rm SI})$ plane, where $m_{\tilde\chi_1^0}$ is the mass of the lightest neutralino and $\sigma_p^{\rm SI}$ is the spin-independent dark matter scattering cross section. As could be expected, we find larger values of $m_{\tilde g}, m_{\tilde q_R}, m_{\tilde\chi_1^0}$ and $m_{\tilde\tau_1}$ than in our pre-LHC M_h fit, and smaller values of $\sigma_p^{\rm SI}$, though BR$(B_s \to \mu^+\mu^-)$ is little affected.

Since $M_h \simeq 125$ GeV is the value that was favored in the CMSSM/NUHM1 fits omitting the $(g-2)_\mu$ constraint [3], we also show some results for fits where $(g-2)_\mu$ is dropped. In this case, we find that preferred regions of the $(m_0, m_{1/2})$ planes are localized at relatively high values, corresponding to relatively large sparticle masses. Correspondingly, the spin-independent dark matter scattering cross section $\sigma_p^{\rm SI}$ would be relatively small in this case, though again there would be relatively little effect on BR$(B_s \to \mu^+\mu^-)$.

Finally, we show selected results for a hypothetical measurement of $M_h \simeq 119$ GeV.

2 Prediction for M_h

We recall that the independent parameters of the CMSSM [58–81] may be taken as the common values of the scalar and fermionic supersymmetry-breaking masses $m_0, m_{1/2}$ at the GUT scale, the supposedly universal trilinear soft supersymmetry-breaking parameter, A_0, and the ratio of Higgs v.e.v.'s, $\tan\beta$. A study of the distribution of Higgs masses in the CMSSM was performed in [82]. Motivated by $(g-2)_\mu$ and, to a lesser extent, BR$(b \to s\gamma)$, we assume that the Higgs mixing parameter $\mu > 0$. In the case of the NUHM1 [83–85], we relax the universality assumption for the soft supersymmetry-breaking contributions to the two Higgs masses, $m_{H_u}^2 = m_{H_d}^2$, allowing $m_{H_u}^2 = m_{H_d}^2 \neq m_0^2$.

In our previous papers [3, 19–25] we constructed a global likelihood function that receives contributions from electroweak precision observables, B-decay measurements, the XENON100 direct search for dark matter scattering [86] and the LHC searches for supersymmetric signals, calculated within the `MasterCode` framework [26]. This incorporates code based on [87, 88] as well as `SoftSUSY` [89], `FeynHiggs 2.8.6` [13–17], `SuFla` [90, 91], `SuperIso` [92–95], `MicrOMEGAs` [96–98] and `SSARD` [99], using the SUSY Les Houches Accord [100, 101]. As before, we use a Markov Chain Monte Carlo (MCMC) approach to sample the parameter spaces of supersymmetric models, and the results of this paper are based on the sample of 70M CMSSM points and another 125M NUHM1 points, both extending up to $m_0, m_{1/2} = 4000$ GeV.

We used in [3] the public results of searches for supersymmetric signals using ∼1/fb of LHC data analyzed by the ATLAS and CMS Collaborations and ∼0.3/fb of data analyzed by the LHCb Collaboration. These include searches for jets $+ \not{E}_T$ events without leptons by ATLAS [102] and CMS [103], searches for the heavier MSSM Higgs bosons, H/A [50, 51], and new upper limits on BR$(B_s \to \mu^+\mu^-)$ from the CMS [104], LHCb [105, 106] and CDF Collaborations [107, 108]. Our global frequentist fit [3] yielded regions of the CMSSM and NUHM1 parameter spaces that are preferred at the 68 and 95 % CL.

This was the basis in [3] for the predictions $M_h = 119.1^{+3.4}_{-2.9}$ GeV in the CMSSM and $M_h = 118.8^{+2.7}_{-1.1}$ GeV in the NUHM1, if the $(g-2)_\mu$ constraint is included as calculated using the `FeynHiggs` code which is quoted as having a theoretical error ± 1.5 GeV [13–17]. It is important to note that these best-fit values are well above the LEP lower limit and below the Tevatron/LHC upper limit on M_h, which played no role in their determination. Figure 12 of [3] displayed the $\Delta\chi^2$ likelihood functions for the `FeynHiggs` value of M_h in these models as blue lines, with the theoretical error ± 1.5 GeV represented by red bands in these plots. As already noted, these predictions increase to $M_h = 124.8^{+3.4}_{-10.5}$ GeV in the CMSSM

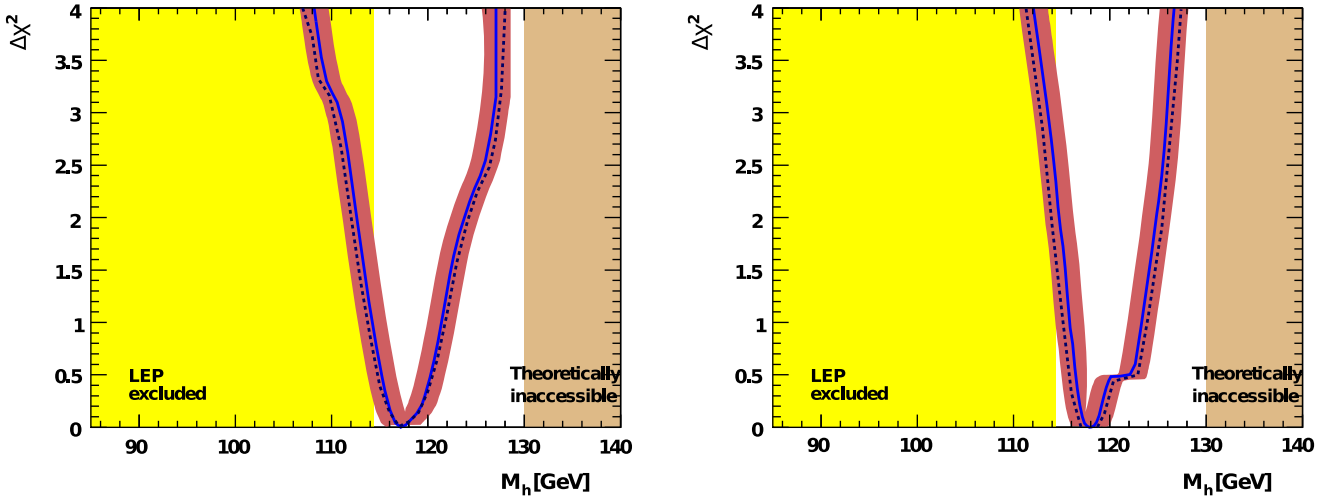

Fig. 1 The one-dimensional $\Delta\chi^2$ functions for M_h in the CMSSM (*left*) and the NUHM1 (*right*). The *solid lines* are for fits including all the available data including $(g-2)_\mu$ but excluding the direct LEP [47, 48], Tevatron [49] and earlier LHC [50, 51] constraints on M_h, with a *red band* indicating the estimated theoretical uncertainty in the calculation of M_h of ∼1.5 GeV. The *dashed line* shows the $\Delta\chi^2$ likelihood function for the nominal central value of a hypothetical LHC measurement of M_h, as estimated on the basis of the frequentist analysis of [3], and allowing for an experimental error of ±1 GeV in the measurement of M_h and a theoretical error of ±1.5 GeV in the `FeynHiggs` calculation of M_h at any given point in the parameter space (Color figure online)

and $126.6^{+0.7}_{-1.9}$ GeV in the NUHM1 if the $(g-2)_\mu$ constraint is dropped. The uncertainty on the M_h prediction is somewhat asymmetric, which is due to the different constraints coming into play. At low M_h values, the most important constraint is that due to the LHC, though other low-energy constraints also play roles. On the other hand, at high values of M_h, it rises logarithmically with the scalar top masses, so increasing M_h increases exponentially the required supersymmetry-breaking mass scales, and worsens the agreement with other low-energy data and the CDM constraint.

2.1 Results without a Higgs-boson mass measurement

Within the supersymmetric frameworks discussed here, a confirmation of the excess reported by ATLAS and CMS [55] and consequently the discovery of a SM-like Higgs boson is expected to be possible in the coming year, with a mass in the range between 114 and 130 GeV [55]. We assume that this measurement will yield a nominal value of M_h within this range, with an experimental error that we estimate as ±1 GeV. We now estimate the one-dimensional likelihood function for the nominal central value of M_h, which may be written as $M_h = M_h^{\rm FH} + \Delta M_h^{\rm Th} + \Delta M_h^{\rm Exp}$, where $M_h^{\rm FH}$ denotes the output of `FeynHiggs` (which was plotted in Fig. 12 of [3] for the fits including $(g-2)_\mu$), $\Delta M_h^{\rm Th}$ denotes its difference from the true value of M_h (the theoretical error estimated as ±1.5 GeV), and $\Delta M_h^{\rm Exp}$ denotes the experimental error in measuring M_h (estimated as ±1 GeV). Here we treat the experimental and the theoretical errors as Gaussians, and include them as supplementary uncertainties in the fit for the nominal central value of M_h. As a consequence of including these uncertainties, the $\Delta\chi^2$ function for the nominal central value of M_h presented here differs slightly from the $\Delta\chi^2$ function for the `FeynHiggs` estimate $M_h^{\rm FH}$ shown in Fig. 12 of [3].

We see in Fig. 1[3] that the values of $\Delta\chi^2$ for the nominal value of M_h calculated in the CMSSM and NUHM1 with the $(g-2)_\mu$ constraint and including both the theoretical and experimental errors lie below the blue lines taken from Fig. 12 of [3]. This is to be expected, since the calculation of the dashed line incorporates additional uncertainties. As is also to be expected, in each case the calculated $\Delta\chi^2$ lies within the previous red band. The most likely nominal value of the LHC measurement of M_h remains $M_h \simeq 119$ GeV in both the CMSSM and NUHM1. A value of $M_h \simeq 125$ GeV is disfavored in our analysis by $\Delta\chi^2 = 2.2$ in the CMSSM and by 1.6 in the NUHM1 if $(g-2)_\mu$ is included. For comparison, a nominal value of $M_h = 114$ GeV, corresponding roughly to the lower limit set by LEP for an SM-like Higgs boson [47, 48], has $\Delta\chi^2 = 0.8(1.5)$. On the other hand, if we drop $(g-2)_\mu$ there is essentially no χ^2 price to be paid by including a measurement of $M_h \simeq 125$ GeV.

[3] The 'theoretically inaccessible' area of $M_h > 130$ GeV could in principle be extended to higher values if one extended the scanned ranges of $m_{1/2}$ and m_0, which are both restricted here to below ∼4 TeV, as discussed above. However, due to the logarithmic dependence of M_h, one would gain only about one GeV even if values up to 10 TeV were included.

3 Implementation of the LHC constraint on M_h

We now study the possibility that the LHC experiments confirm the excess reported around 125 GeV and indeed discover a SM-like Higgs boson. Assuming

$$M_h = 125 \pm 1 \text{ (exp.)} \pm 1.5 \text{ (theo.) GeV}, \quad (1)$$

we incorporate this new constraint using the 'afterburner' approach discussed previously [3] for other observables. This value would be favored if $(g-2)_\mu$ were dropped from our global CMSSM or NUHM1 fit [3]. Alternatively, a measurement of such a high M_h value could point to the realization of some different (possibly GUT-based) version of the MSSM (see, for instance, [109]). We also mention briefly some implications if $M_h \simeq 119$ GeV.

3.1 Comments on the LHC data

As a preamble to these studies, we first comment on the results of the current ATLAS/CMS Higgs combination. We recall that the *local* p-value for the background-only hypothesis for the excess found in the ATLAS data at $M_h \simeq 125$ GeV is $p = 1.9 \times 10^{-4}$, while that in the CMS data at $M_h \simeq 125$ GeV has $p = 5 \times 10^{-3}$. In addition, CMS reports an excess in the ZZ^* channel at $M_h = 119$ GeV with similar significance, but this is not confirmed by ATLAS.

In order to assess the *global* p-value of a potential signal, one should take the 'look-elsewhere effect' (LEE) into account. This is conventionally estimated by adding to the *local* p-value the quantity $N \times \exp(-Z^2_{\rm max}/2)$, where N is the number of times the observed upper limit on the signal crosses over the $\mu = \sigma/\sigma_{\rm SM} = 0$ level in the upward direction, and $Z_{\rm max}$ is the maximal signal significance [55]. Accounting for the LEE, ATLAS assess the *global* p-value of their excess at 125 GeV In the range (110, 146) GeV to be 0.6 %, and CMS assess the significance of their excess at 125 GeV to be 1.9 % in the range (110, 145) GeV.

On the other hand, as the CMSSM and NUHM1 naturally require $M_h \lesssim 130$ GeV, the LEE factor is strongly reduced in these frameworks.

Since the excess around 125 GeV is common to both experiments and has the correct signal strength: $\mu \approx 1$ can be interpreted as a Higgs signal in either the SM or a supersymmetric framework. We focus here on this interpretation, commenting subsequently on some implications if $M_h \simeq 119$ GeV.

3.2 What if $M_h = 125$ GeV?

We first examine the effects on the global likelihood functions in various CMSSM and NUHM1 parameter planes, and then study implications for various observables of a potential LHC measurement $M_h \simeq 125$ GeV, see Eq. (1). The $(m_0, m_{1/2})$ planes shown in Fig. 2 are for the CMSSM (left) and NUHM1 (right).[4] The regions preferred at the 68 % CL are outlined in red, and those favored at the 95 % CL are outlined in blue. The solid (dotted) lines include (omit) the assumed LHC Higgs constraint. The open green star denotes the pre-Higgs best-fit point [3], whereas the solid green star indicates the new best-fit point incorporating a Higgs-boson mass measurement at 125 GeV.

Since in the CMSSM and NUHM1 the radiative corrections contributing to the value of M_h are sensitive primarily to $m_{1/2}$ and $\tan\beta$, and only to a lesser extent to m_0 (the stop masses, which are the most relevant for M_h, depend mostly on $m_{1/2}$ due to the RGE running, and only mildly on m_0), we expect that the primary effect of imposing the M_h constraint should be to affect the preferred ranges of $m_{1/2}$ and $\tan\beta$, with a lesser effect on the preferred range of m_0. This effect is indeed seen in both panels of Fig. 2. We see that the 68 % CL ranges of $m_{1/2}$ extend to somewhat larger values and with a wider spread than the pre-Higgs results, particularly in the NUHM1. However, the NUHM1 best-fit value of $m_{1/2}$ remains at a relatively low value of ∼800 GeV, whereas the best-fit value of $m_{1/2}$ in the CMSSM moves to ∼1900 GeV. This jump reflects the flatness of the likelihood function for $m_{1/2}$ between ∼700 GeV and ∼2 TeV, which is also reflected later in the one-dimensional $\Delta\chi^2$ functions for some sparticle masses.[5]

When we add the hypothetical M_h constraint the total χ^2 at the best-fit points increases substantially, as seen in Table 1, and the p-value decreases correspondingly. The table compares fit probabilities for two different assumptions on the Higgs boson mass measurements ≃119, 125 GeV, see above, and with the option of dropping the $(g-2)_\mu$ constraint in the latter case.[6] The combination of the increase in χ^2 and in the increase in the number of d.o.f. leads to a substantially lower p-value after the inclusion of Eq. (1), if $(g-2)_\mu$ is taken into account. On the other hand, a hypothetical mass measurement at 119 GeV would yield an

[4] We have omitted from the NUHM1 sample displayed here and in subsequent figures a grouping of points at large $m_{1/2}$ and small m_0 for which different codes yield discrepant values of the relic density. `MicrOMEGAs` [96–98] and `DarkSusy` [110, 111] yield densities within the WMAP range for these points, whereas `SuperIso Relic` (see [95]) and `SSARD` [99] both yield substantially lower densities. The other figures shown in this paper are not affected significantly by the omission of these points (which have $\Delta\chi^2 > 5$), pending resolution of this discrepancy. Tests in other regions of the NUHM1 sample have not revealed significant discrepancies between these codes.

[5] Our fits are relatively insensitive to A_0, so we do not display figures for this parameter.

[6] The fit probabilities are indicative of the current experimental data preferences for one scenario over another but, as discussed in [3], but they do not provide a robust confidence-level estimation for the actual choice made by Nature.

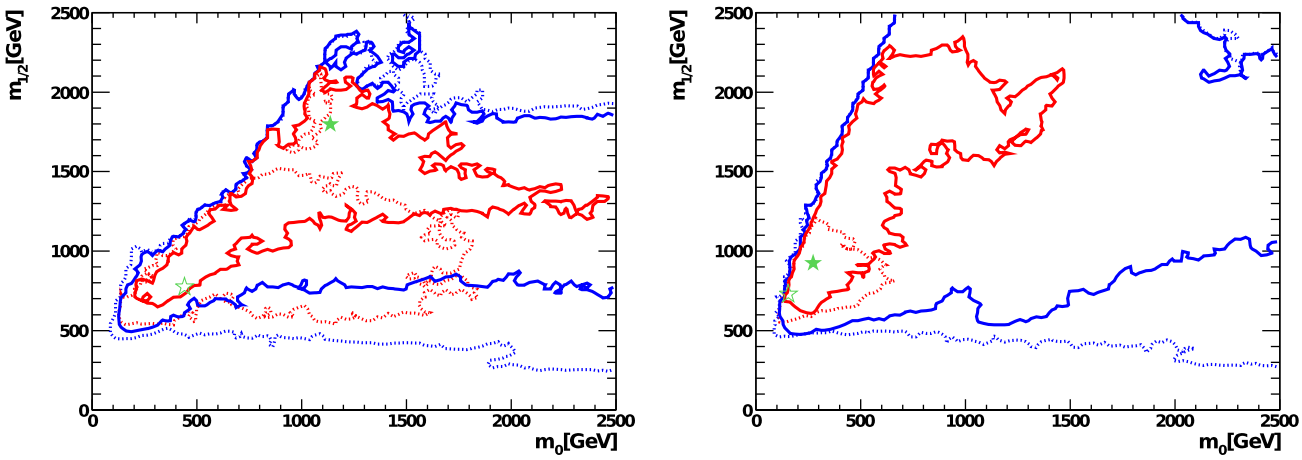

Fig. 2 The $(m_0, m_{1/2})$ planes in the CMSSM (*left*) and the NUHM1 (*right*). The $\Delta\chi^2 = 2.30$ and 5.99 contours, commonly interpreted as the boundaries of the 68 and 95 % CL regions, are indicated in *red* and *blue*, respectively, the solid lines including the hypothetical LHC measurement $M_h = 125 \pm 1$ GeV and allowing for a theoretical error ± 1.5 GeV, and the *dotted lines* showing the contours found previously in [3] without this M_h constraint. Here the *open green stars* denote the pre-Higgs best-fit points [3], whereas the *solid green stars* indicate the new best-fit points (Color figure online)

Table 1 Comparison of the best-fit points found in the CMSSM and NUHM1 pre-Higgs [3] and for the two potential LHC Higgs mass measurements discussed in the text: $M_h \simeq 119$ and 125 GeV. In the latter case, we also quote results if the $(g-2)_\mu$ constraint is dropped. At the best-fit NUHM1 points, the common values of the soft supersymmetry-breaking contributions to the Higgs squared masses are the following pre-Higgs: -1.2×10^6 GeV^2, with $M_h \simeq 125$ GeV and $(g-2)_\mu$: -5.5×10^6 GeV^2, with $M_h \simeq 125$ GeV but without $(g-2)_\mu$: -8.6×10^5 GeV^2, with $M_h \simeq 119$ GeV and $(g-2)_\mu$: -1.2×10^6 GeV^2

Model	Minimum χ^2/d.o.f.	Fit Probability	$m_{1/2}$ (GeV)	m_0 (GeV)	A_0 (GeV)	$\tan\beta$
CMSSM						
pre-Higgs	28.8/22	15 %	780	440	−1120	40
$M_h \simeq 125$ GeV, $(g-2)_\mu$	31.0/23	12 %	1800	1140	1370	46
$M_h \simeq 125$ GeV, no $(g-2)_\mu$	21.3/22	50 %	1830	1320	−1860	47
$M_h \simeq 119$ GeV	28.9/23	18 %	880	400	−890	38
NUHM1						
pre-Higgs	26.9/21	17 %	730	150	−910	41
$M_h \simeq 125$ GeV, $(g-2)_\mu$	28.9/22	15 %	920	270	1730	27
$M_h \simeq 125$ GeV, no $(g-2)_\mu$	19.7/21	52 %	2060	1400	2610	46
$M_h \simeq 119$ GeV	27.1/22	20 %	750	150	−420	34

improvement in the fit. For comparison, we also show the parameters for the best-fit points. Since the uncertainties are large and highly non-Gaussian, we omit them from the table.

The restrictions that the hypothetical LHC M_h constraint imposes on $m_{1/2}$ are also visible in Fig. 3, where we display the effects of an LHC M_h constraint in the $(m_{1/2}, \tan\beta)$ planes of the CMSSM and NUHM1. We see here that an LHC M_h constraint enlarges visibly the 68 % CL range of $\tan\beta$ in the NUHM1, whereas the change is less pronounced in the CMSSM.

The results for the $(M_A, \tan\beta)$ planes in the CMSSM and the NUHM1 are shown in Fig. 4. We observe a strong increase in the best-fit value of M_A in both models, especially in the CMSSM, where now $M_A \sim 1600$ GeV is preferred. We re-emphasize, however, that the likelihood function varies relatively slowly in both models, as compared to the pre-LHC fits.

We now discuss the CMSSM and NUHM1 predictions for some of the most interesting supersymmetric observables for the LHC in light of a possible LHC measurement at $M_h \simeq 125$ GeV.

The upper panels of Fig. 5 display the one-dimensional $\Delta\chi^2$ functions for $m_{\tilde{g}}$ before and after applying the new LHC $M_h \simeq 125$ GeV constraint (dashed and solid lines, re-

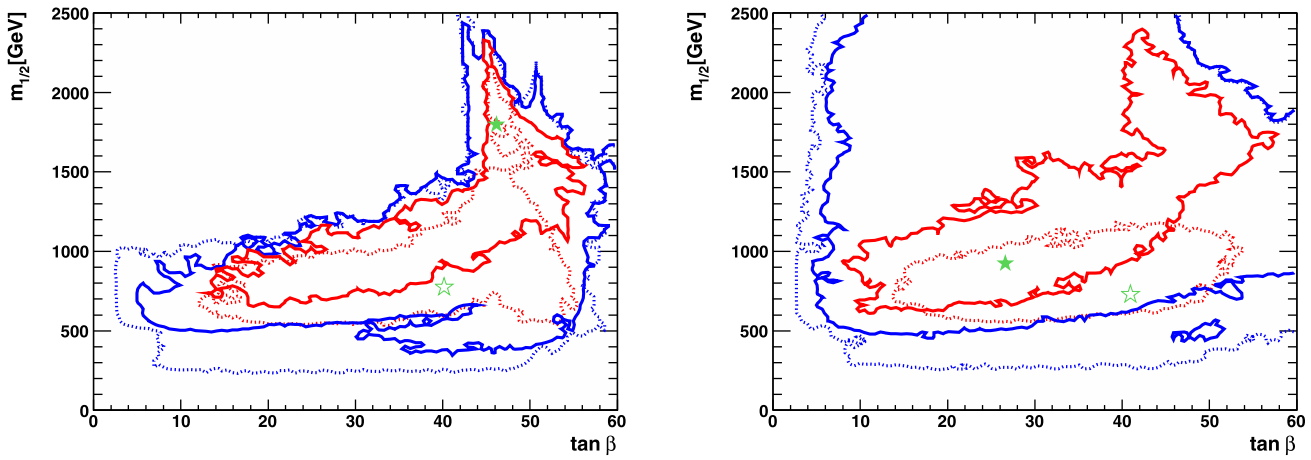

Fig. 3 The $(m_{1/2}, \tan\beta)$ planes in the CMSSM (*left*) and the NUHM1 (*right*), for $M_h \simeq 125$ GeV. The notations and significations of the contours are the same as in Fig. 2

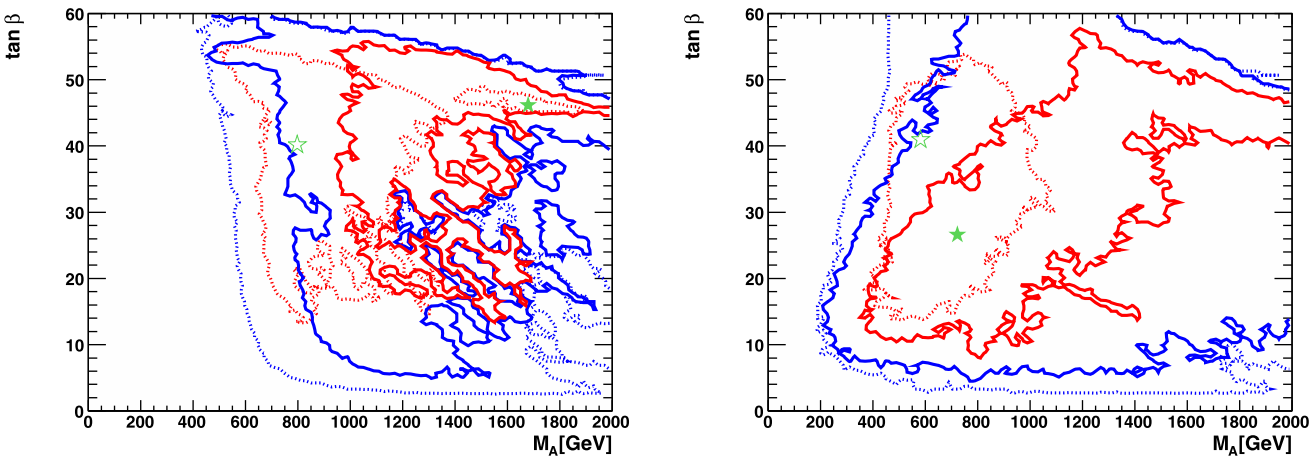

Fig. 4 The $(M_A, \tan\beta)$ planes in the CMSSM (*left*) and the NUHM1 (*right*), for $M_h \simeq 125$ GeV. The notations and significations of the contours are the same as in Fig. 2

spectively, in both cases including $(g-2)_\mu$). We also show as dotted lines the $\Delta\chi^2$ functions for a fit including $M_h \simeq 125$ GeV and dropping $(g-2)_\mu$. As expected on the basis of Fig. 2, the preferred values $m_{\tilde{g}} \sim 4$ TeV in the CMSSM are much higher than in our pre-LHC fit and what would be preferred if $M_h \simeq 119$ GeV, and presumably beyond the reach of the LHC. On the other hand, in the NUHM1 $m_{\tilde{g}} \sim 2$ TeV is marginally preferred. However, in both models the $\Delta\chi^2$ function varies little over the range (2, 4) TeV. Similar features are found for $m_{\tilde{q}_R}$, as shown in the lower panels of Fig. 5. In both models, the regions of $m_{\tilde{g}}$ and $m_{\tilde{q}_R}$ with $\Delta\chi^2 \lesssim 1$ start at masses around 1.5 TeV, leaving a large range accessible to the SUSY searches at the LHC. In the case of the lighter stau mass $m_{\tilde{\tau}_1}$ for $M_h \simeq 125$ GeV shown in Fig. 6, we again see preferred masses larger than in the pre-Higgs fit, with favored values extending up to $m_{\tilde{\tau}_1} \sim 1$ TeV.

We now turn to the predictions of our fits for BR$(B_s \to \mu^+\mu^-)$, shown in Fig. 7. This observable is not very sensitive directly to M_h, and the indirect sensitivity via $m_{1/2}$ is not very strong, though smaller values of $m_{1/2}$ do lead to larger values of BR$(B_s \to \mu^+\mu^-)$, in general. As seen in Fig. 7, imposing the putative LHC M_h constraint indeed has little effect on BR$(B_s \to \mu^+\mu^-)$. We recall that the best-fit values in the CMSSM and NUHM1 are both slightly larger than in the SM, and enhancements of up to $\mathcal{O}$(30–40 %) with respect to the SM prediction could be detected at the LHC at the $3\,\sigma$ level.

Finally, in Fig. 8 we show results for the preferred regions in the $(m_{\tilde{\chi}_1^0}, \sigma_p^{\rm SI})$ plane. As seen in Fig. 8, the fact that larger values of $m_{1/2}$ and hence $m_{\tilde{\chi}_1^0}$ are favored by the larger values of M_h implies that at the 68 % CL the preferred range of $\sigma_p^{\rm SI}$ is significantly lower when $M_h \simeq 125$ GeV, when compared to our previous best fit with $M_h = 119$ GeV, ren-

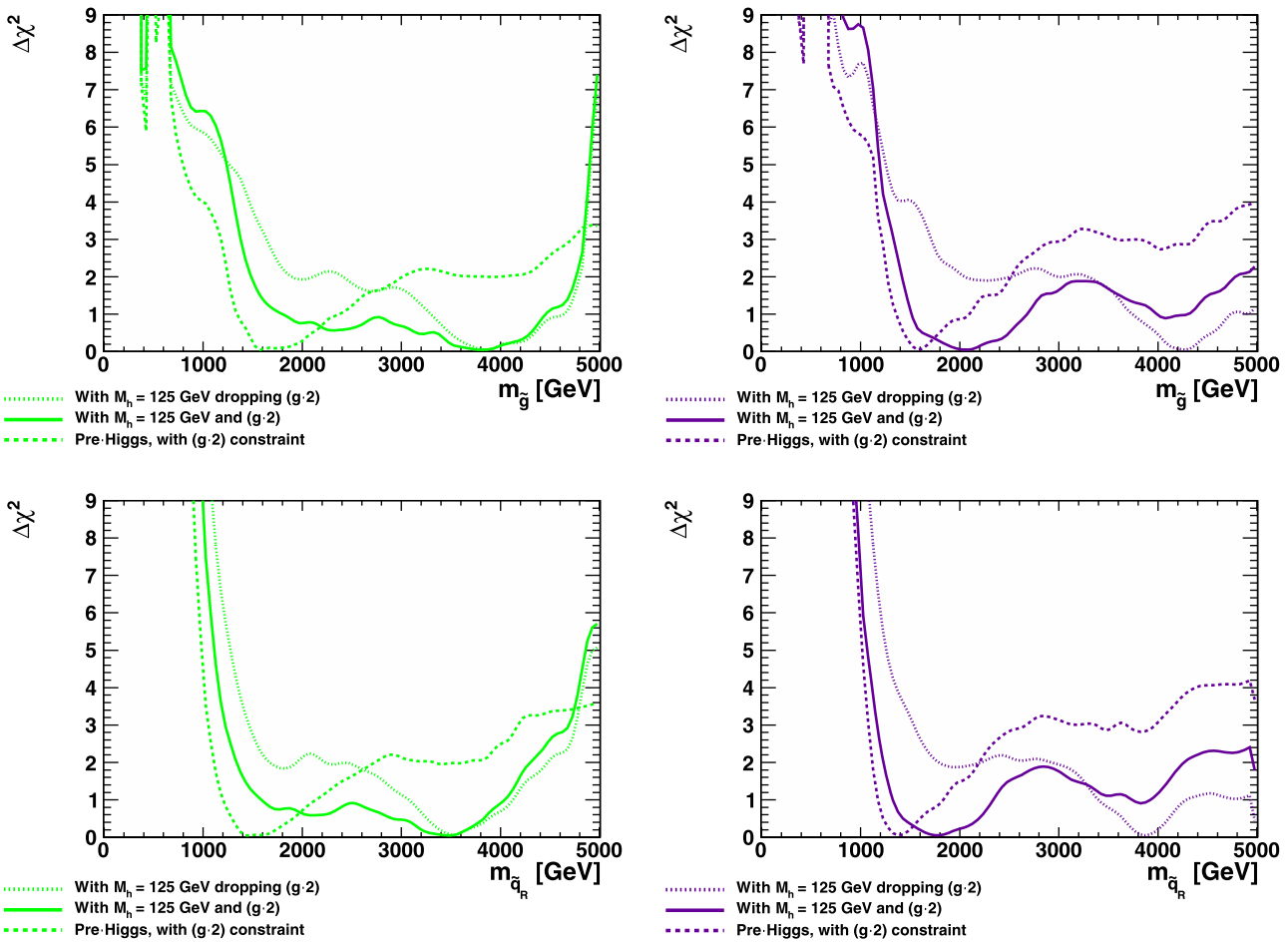

Fig. 5 The one-dimensional $\Delta\chi^2$ functions for $m_{\tilde{g}}$ (*upper*) and $m_{\tilde{q}_R}$ (*lower*) in the CMSSM (*left*) and the NUHM1 (*right*). The *solid lines* are for fits assuming $M_h \simeq 125$ GeV and including $(g-2)_\mu$, and the *dotted lines* for fits with $M_h \simeq 125$ GeV but without $(g-2)_\mu$. The *dashed lines* show the results for fits without $M_h \simeq 125$ GeV but including $(g-2)_\mu$ [3]

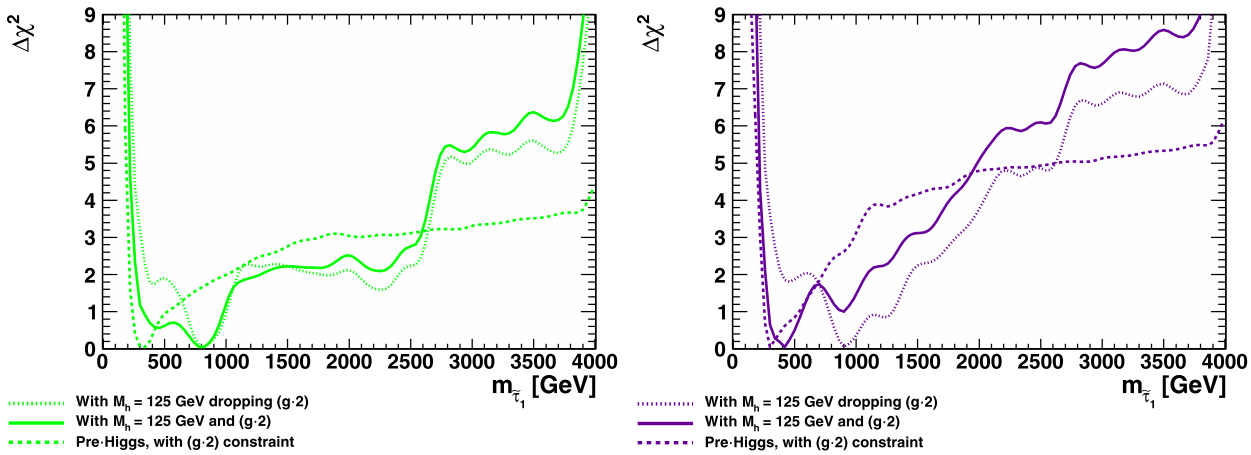

Fig. 6 The one-dimensional $\Delta\chi^2$ functions for the lighter scalar tau mass $m_{\tilde{\tau}_1}$ in the CMSSM (*left*) and the NUHM1 (*right*), for $M_h \simeq 125$ GeV. The notations and significations of the *lines* are the same as in Fig. 5

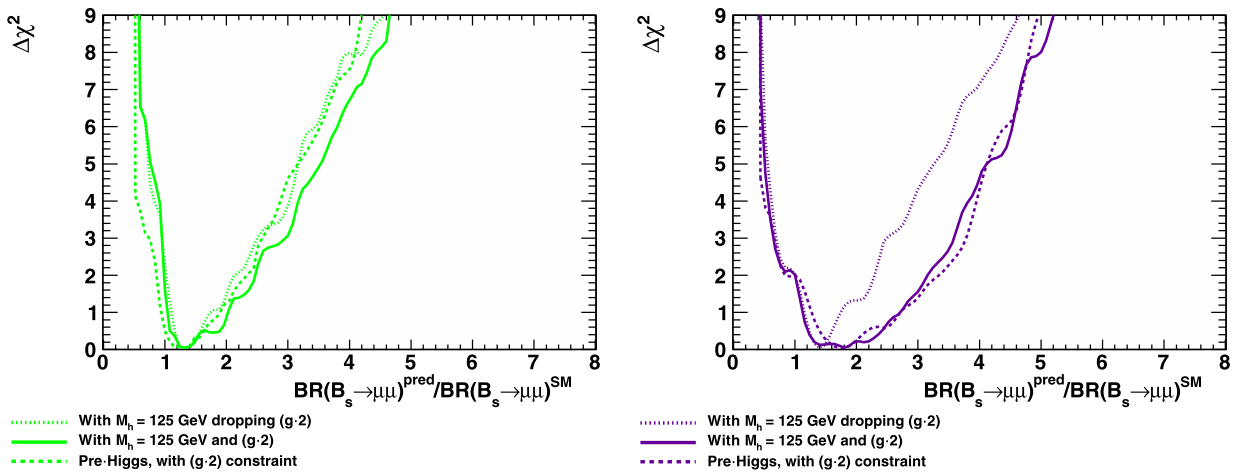

Fig. 7 The one-dimensional $\Delta\chi^2$ functions for BR$(B_s \to \mu^+\mu^-)$ in the CMSSM (*left*) and the NUHM1 (*right*), for $M_h \simeq 125$ GeV. The notations and significations of the *lines* are the same as in Fig. 5

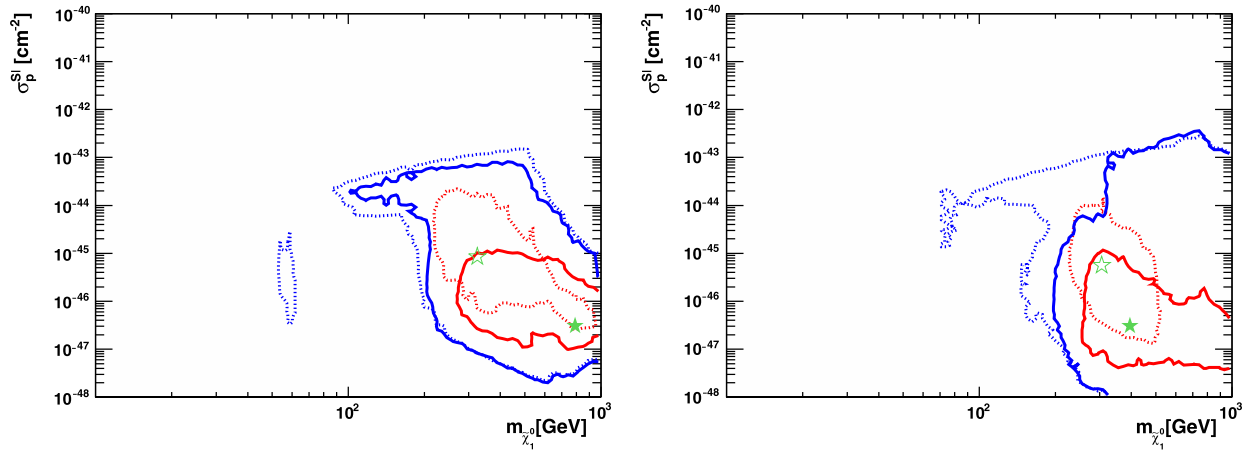

Fig. 8 The $(m_{\tilde{\chi}_1^0}, \sigma_p^{\rm SI})$ planes in the CMSSM (*left*) and the NUHM1 (*right*), for $M_h \simeq 125$ GeV. The notations and significations of the *contours* are the same as in Fig. 2

dering direct detection of dark matter significantly more difficult. Again, this effect on $m_{\tilde{\chi}_1^0}$ is more pronounced in the CMSSM, whereas in the NUHM1 the value of $m_{\tilde{\chi}_1^0}$ for the best-fit point changes only slightly.

3.3 Results dropping the $(g-2)_\mu$ constraint

We have restricted our attention so far to $M_h \simeq 125$ GeV assuming the $(g-2)_\mu$ constraint. However, this value of M_h corresponds approximately to our best-fit points in [3] when the $(g-2)_\mu$ constraint is dropped.[7] Accordingly, we now consider the same measurement as given in Eq. (1), but with $(g-2)_\mu$ dropped from the fit.[8] In the following plots we show results for fits omitting $(g-2)_\mu$, pre-Higgs (dotted) and post-Higgs (solid).

We see in Fig. 9 that the regions of the $(m_0, m_{1/2})$ planes in the CMSSM and NUHM1 that are favored at the 68 % CL are concentrated at large values if the $(g-2)_\mu$ constraint is dropped. This reflects the relative harmony between the LHC $\not{E}_T$ constraints and the hypothetical $M_h \simeq 125$ GeV measurement if $(g-2)_\mu$ is omitted. The inclusion of Eq. (1) substantially sharpens the prediction at the 68 % CL, whereas it is less pronounced for the 95 % CL contours.

[7] We recall that it was shown in [3] that the CMSSM/NUHM1 interpretation of $(g-2)_\mu$ is in some tension with the LHC constraints on events with $\not{E}_T$.

[8] There are small differences between the pre-Higgs 68 and 95 % CL contours presented here and the corresponding contours in [3], which provide a measure of the uncertainties in the interpretation of the MCMC data generated for our analysis.

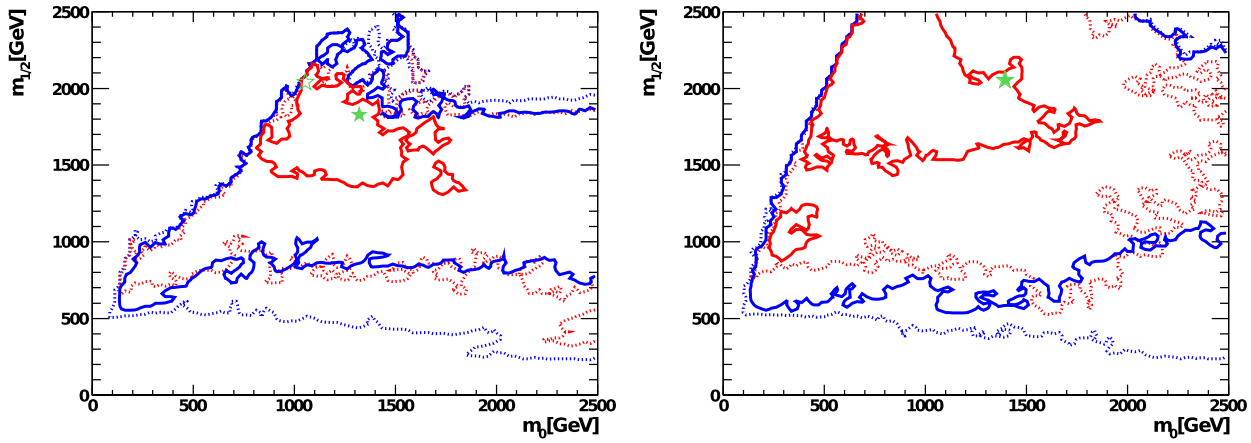

Fig. 9 The $(m_0, m_{1/2})$ planes in the CMSSM (*left*) and the NUHM1 (*right*), for $M_h \simeq 125$ GeV, but dropping the $(g-2)_\mu$ constraint. *Dotted lines* show the contours found previously in [3] dropping the $(g-2)_\mu$ but without this M_h constraint. Here the *open green stars* denote the pre-Higgs best-fit points [3] (also dropping $(g-2)_\mu$), whereas the *solid green stars* indicate the new best-fit points. These best-fit points are essentially coincident in the NUHM1 case (Color figure online)

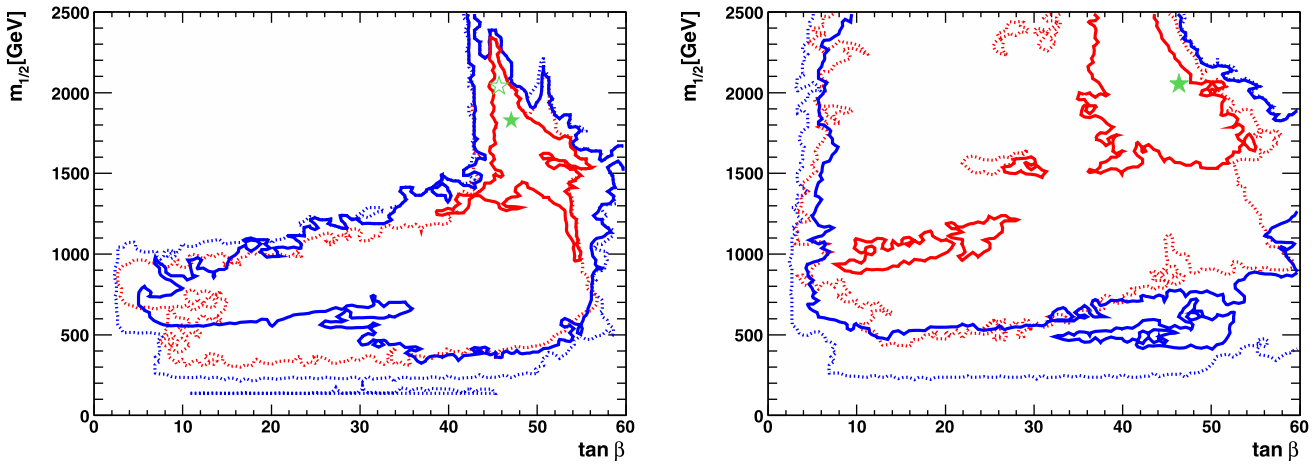

Fig. 10 The $(m_{1/2}, \tan\beta)$ planes in the CMSSM (*left*) and the NUHM1 (*right*), for $M_h \simeq 125$ GeV, but dropping the $(g-2)_\mu$ constraint. The notations and significations of the *contours* are the same as in Fig. 9

As we see in Fig. 10, the concentration at relatively large $m_{1/2}$ is reflected in a correlated preference for large values of $\tan\beta$. Furthermore, as seen in Fig. 11, the corresponding preferred range of M_A is also concentrated at relatively large masses. Again the inclusion of Eq. (1) considerably sharpens the preferred parameter ranges.

Looking back now at the one-dimensional $\Delta\chi^2$ functions for the fits without $(g-2)_\mu$ that are shown as dotted lines in Figs. 5 and 6, we see that the preference for large values of $(m_0, m_{1/2})$ carries over into relatively large values of $m_{\tilde{g}}, m_{\tilde{q}_R}$ and $m_{\tilde{\tau}_1}$. In particular, the $(g-2)_\mu$-less scenarios offer somewhat gloomy prospects for sparticle detection at the LHC. On the other hand, as seen in Figs. 7, there is little change in the prediction for $\mathrm{BR}(B_s \to \mu^+\mu^-)$ if $(g-2)_\mu$ is omitted.

Turning finally to the predictions for σ_p^{SI} if $(g-2)_\mu$ is omitted, shown in Fig. 12, we see that the relatively large values of $m_{1/2}$ seen in Fig. 9 are reflected in relatively large values of $m_{\tilde{\chi}_1^0}$, which correspond in turn to relatively low values of σ_p^{SI}. The inclusion of Eq. (1) again strongly reduces the preferred parameter ranges.

An alternative interpretation of a Higgs signal around $M_h \simeq 125$ GeV would be that while the MSSM might still be realized, it is not the CMSSM nor the NUHM1 that describes Nature correctly, but another version of the MSSM. In this case, the prospects for sparticle detection at the LHC and dark matter detection might well be more cheerful than in the $(g-2)_\mu$-less CMSSM and NUHM1 scenarios discussed here. However, the exploration of such possible alternative models lies beyond the scope of our analysis.

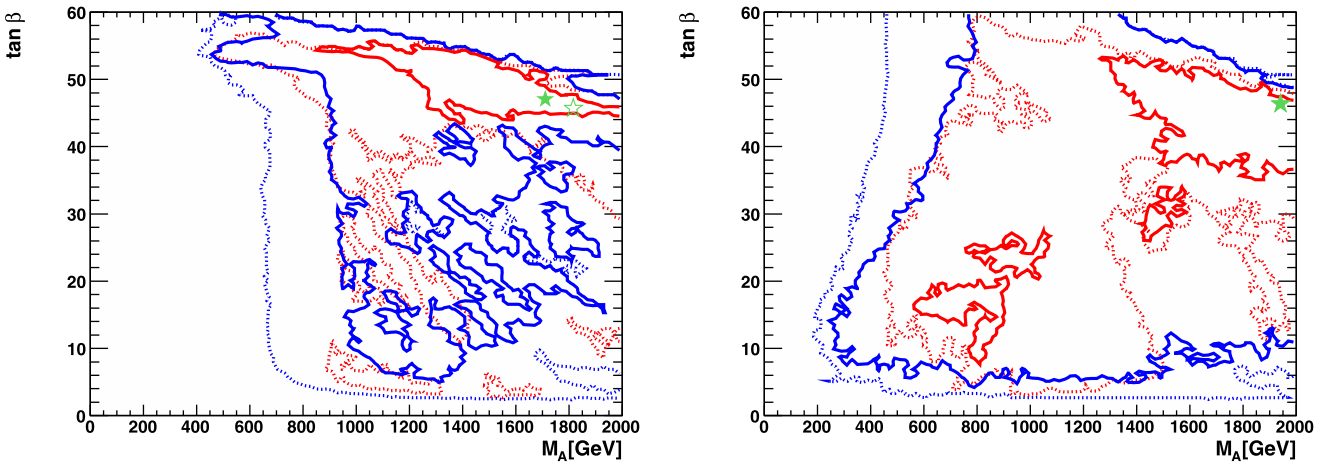

Fig. 11 The $(M_A, \tan\beta)$ planes in the CMSSM (*left*) and the NUHM1 (*right*), for $M_h \simeq 125$ GeV, but dropping the $(g-2)_\mu$ constraint. The notations and significations of the *contours* are the same as in Fig. 9

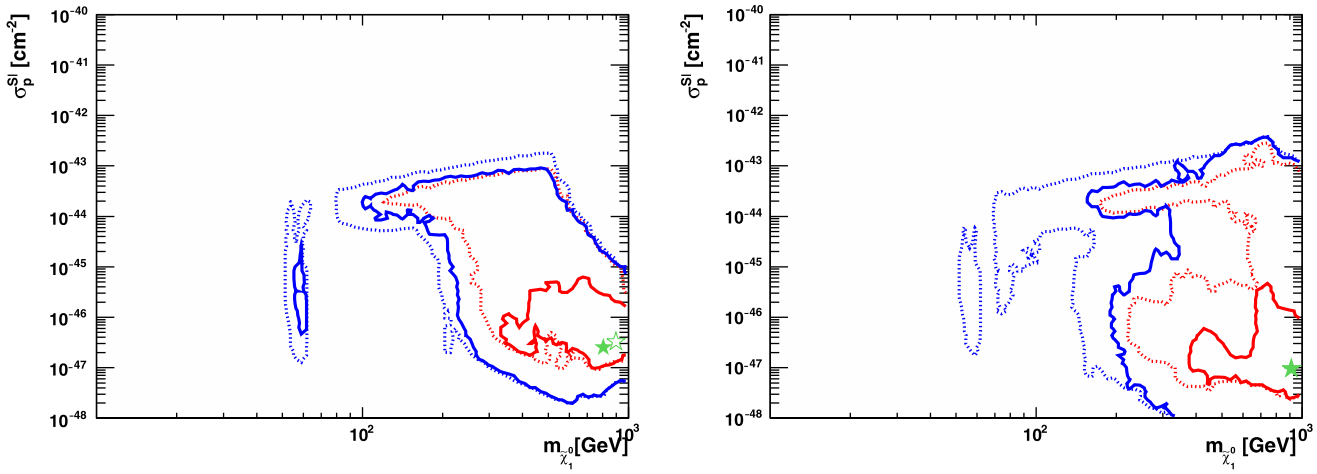

Fig. 12 The $(m_{\tilde{\chi}_1^0}, \sigma_p^{\rm SI})$ planes in the CMSSM (*left*) and the NUHM1 (*right*), for $M_h \simeq 125$ GeV, but dropping the $(g-2)_\mu$ constraint. The notations and significations of the *contours* are the same as in Fig. 9

3.4 What if $M_h = 119$ GeV?

We have restricted our attention so far to $M_h \simeq 125$ GeV, which corresponds to the excess seen in both CMS and ATLAS. We now consider an alternative potential LHC measurement $M_h = 119 \pm 1$ GeV, which corresponds to the CMS ZZ^* signal and our earlier predictions including the $(g-2)_\mu$ constraint, again allowing for a theoretical error ± 1.5 GeV in the calculation of M_h for any given set of CMSSM or NUHM1 parameters.

The $(m_0, m_{1/2})$ planes shown in Fig. 13 for the CMSSM (left) and NUHM1 (right), the preferred regions are shown at the 68 % CL (red) and 95 % CL, with the solid (dotted) lines include (omit) the assumed LHC Higgs constraint. Since this assumed LHC value of M_h coincides with the previous best-fit values in both the CMSSM and NUHM1, the best-fit points in these models (indicated by the green stars in Fig. 13) are nearly unaffected by the imposition of the putative LHC constraint. The effect of the hypothetical measurement restricting the range in $m_{1/2}$ is indeed seen in both panels of Fig. 13, though for the 68 % CL contour (shown in red) it is much more pronounced for the CMSSM than for the NUHM1, whereas for the 95 % CL contour (shown in blue) it is more significant for the NUHM1. This reflects the fact in the NUHM1 the global $\Delta\chi^2$ function found in [3] rose quite steeply in the neighborhood of the best-fit point, resulting in a relatively tight 68 % CL contour, whereas the rise of χ^2 away from the best-fit point in the CMSSM was more gradual. This led previously to a larger 68 % CL contour and a broader range of M_h at the 68 % CL, which is now more affected by an assumed LHC M_h constraint. On the other hand, the 95 % CL contour in the NUHM1 extended previously to larger values of $m_{1/2}$ than in the CMSSM, and

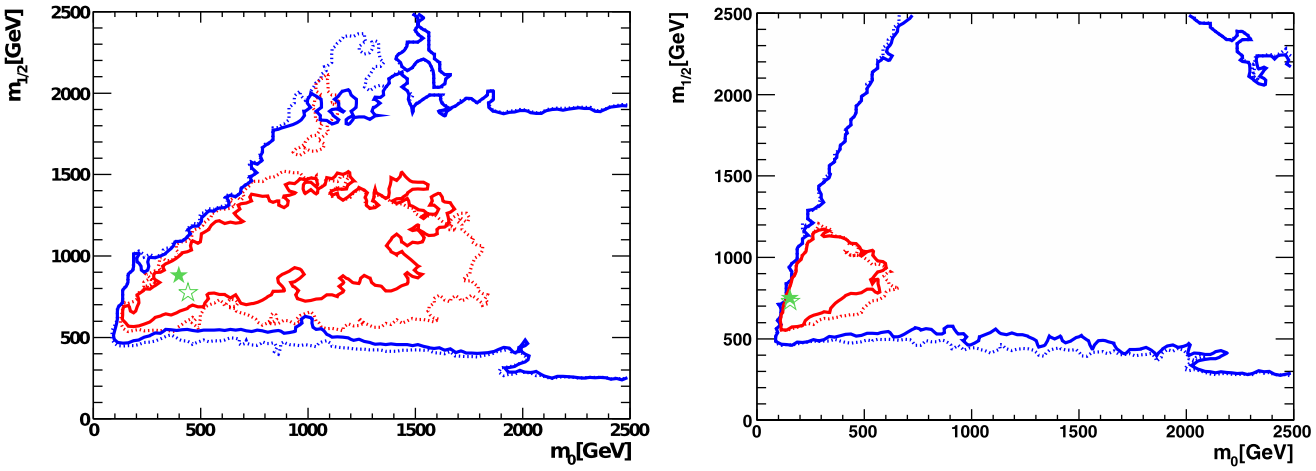

Fig. 13 The $(m_0, m_{1/2})$ planes in the CMSSM (*left*) and the NUHM1 (*right*) assuming a hypothetical measurement of $M_h = 119$ GeV. The notations and significations of the *contours* are the same as in Fig. 2

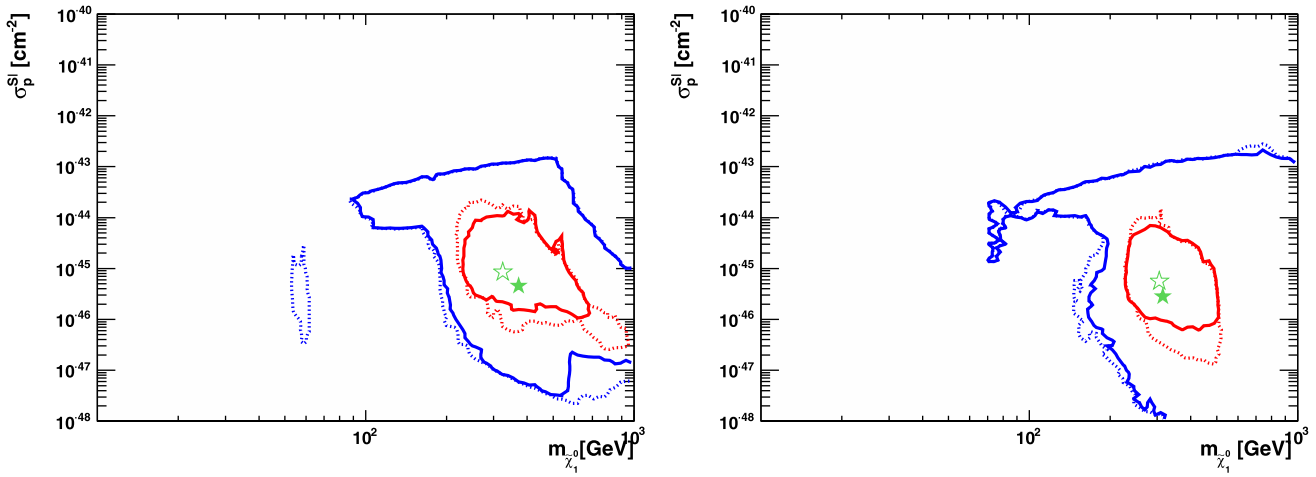

Fig. 14 The $(m_{\tilde{\chi}_1^0}, \sigma_p^{\mathrm{SI}})$ planes in the CMSSM (*left*) and the NUHM1 (*right*), for $M_h \simeq 119$ GeV. The notations and significations of the *contours* are the same as in Fig. 13

these values are particularly susceptible to the LHC M_h constraint.

Although we add another constraint (as discussed above), the total χ^2 at the best-fit points do not change.[9] For this reason, the p-values for the CMSSM and NUHM1 would increase for a hypothetical measurement $M_h \simeq 119$ GeV, corresponding formally to better overall fits to the larger data set, as seen in Table 1.

As one might expect, such an LHC M_h constraint would reduce considerably the 68 % CL range of $\tan\beta$ in the CMSSM. This is because, for $m_{1/2}$ close to the best-fit value, ∼700 to 800 GeV, fixing the Higgs mass at 119 GeV disfavors low values of $\tan\beta$, which yield low values of M_h. This effect is not important in the NUHM1, where the range of $\tan\beta$ was already smaller before imposing the M_h constraint. We also note that M_A is restricted to somewhat smaller values when the hypothetical LHC constraint on M_h is included. Furthermore, as expected, the values of $m_{\tilde{g}}$ at the minima of the χ^2 functions are not affected and there is little change in χ^2 for $m_{\tilde{g}}$ between 2 and 3 TeV. (The corresponding plots are not shown.) However, there are significant effects at both lower and higher values of $m_{\tilde{g}}$. In particular, large values of $m_{\tilde{g}} \gtrsim 3$ TeV are disfavored. The prospects for discovering gluinos at the LHC in the near future would remain uncertain in both the CMSSM and NUHM1. An LHC measurement of $M_h \simeq 119$ GeV would disfavor large squark masses, but the 95 % CL range would still extend to $m_{\tilde{q}_R} \sim 4$ TeV in the CMSSM and ∼2 TeV in the NUHM1. The preferred value of $m_{\tilde{\tau}_1} \sim 300$ GeV in both

[9] They would change only slightly if the Higgs mass were assumed to differ by $\lesssim 1$ GeV from that obtained at the best-fit point.

the CMSSM and NUHM1 both with and without the hypothetical LHC M_h measurement, with large masses again becoming somewhat more disfavored.

Finally, in both the CMSSM and the NUHM1 there is little impact on the 95 % CL regions nor on the 68 % CL region in the NUHM1 in the $(m_{m_{\tilde{\chi}_1^0}}, \sigma_p^{\rm SI})$ plane. The only substantial change, as can be seen in Fig. 14, appears in the 68 % CL region of the CMSSM, where now values of $m_{\tilde{\chi}_1^0} \gtrsim 700$ GeV and $\sigma_p^{\rm SI} \lesssim 10^{-46}$ cm^{-2} are disfavored after the inclusion of a Higgs-boson mass measurement at 119 GeV.

4 Summary and conclusions

The ATLAS and CMS searches for the Higgs boson have already excluded a very large range of masses, with the only remaining windows for a SM-like Higgs boson being in the ranges $M_h \in (115.5, 127)$ GeV or >600 GeV [52–55]. The latter range is disfavored by precision electroweak data, so attention naturally focuses on the low-mass range. It may or not be a coincidence that this range includes the range $M_h \lesssim 130$ GeV accessible in simple supersymmetric models such as the CMSSM and NUHM1. Within this range, our previous global fits of these models including $(g-2)_\mu$ predicted $M_h \sim 119$ GeV if the $(g-2)_\mu$ constraint was included in the fit, and $M_h \sim 126$ GeV if $(g-2)_\mu$ was omitted [3]. The latest ATLAS and CMS results display an interesting fluctuation at $M_h \sim 125$ GeV (i.e. close to the latter result from [3]) and we have combined a hypothetical measurement of $M_h = 125$ GeV with the global likelihood functions obtained in our previous fits [3].

As we have shown in this paper, this combination refines our previous predictions for the CMSSM and NUHM1 model parameters within global fits incorporating $(g-2)_\mu$. In particular, the combination prefers a range of larger values of $m_{1/2}$, resulting in larger values of $m_{\tilde{g}}$ and other sparticle masses being preferred, restricting the prospects for discovering supersymmetry at the LHC within these models. The predictions for $\sigma_p^{\rm SI}$ are pushed to higher masses and lower cross sections, particularly in the CMSSM. There are also smaller changes in the predictions for other observables such as BR$(B_s \to \mu^+\mu^-)$.

We have also shown the analogous CMSSM and NUHM1 fit results for a hypothetical measurement of $M_h \simeq 125$ GeV if the $(g-2)_\mu$ constraint is omitted. In this case we find a stronger preference for larger values of $(m_0, m_{1/2})$, and correspondingly larger values of $\tan\beta$ and M_A, as well as larger values of $m_{\tilde{g}}, m_{\tilde{q}_R}$, potentially lying beyond the reach of the LHC. We have also commented on the potential implications of a hypothetical Higgs discovery at $M_h \simeq 119$ GeV.

Time will soon tell whether the LHC experiments are indeed discovering the Higgs boson. However, we have shown that $M_h = 125$ GeV is a possibility within the CMSSM and NUHM1, although it lies at the upper range of what is possible within the CMSSM or NUHM1, and might suggest reduced prospects for discovering these particular models of supersymmetry at the LHC. Alternatively, it could well be that one should look beyond the frameworks of the models discussed here.

Note added in proof After acceptance of this paper for publication, we became aware of issues in the implementation of the `FeynHiggs` code and in the cold dark matter density calculation, which required extra sampling and reprocessing of the NUHM1 parameter space. We are grateful to Nazila Mahmoudi and Azar Mustafayev for discussions on dark matter density calculations.

Acknowledgements The work of O.B., K.J.D., J.E., J.M. and K.A.O. is supported in part by the London Centre for Terauniverse Studies (LCTS), using funding from the European Research Council via the Advanced Investigator Grant 267352. The work of S.H. is supported in part by CICYT (grant FPA 2010–22163-C02-01) and by the Spanish MICINN's Consolider-Ingenio 2010 Program under grant MultiDark CSD2009-00064. The work of K.A.O. is supported in part by DOE grant DE-FG02-94ER-40823 at the University of Minnesota.

References

1. J.R. Ellis, S. Heinemeyer, K.A. Olive, G. Weiglein, Phys. Lett. B **515**, 348 (2001). arXiv:hep-ph/0105061
2. S. Ambrosanio, A. Dedes, S. Heinemeyer, S. Su, G. Weiglein, Nucl. Phys. B **624**, 3 (2002). arXiv:hep-ph/0106255
3. O. Buchmueller et al., Eur. Phys. J. C **72**, 1878 (2012). arXiv:1110.3568 [hep-ph]
4. J.R. Ellis, G. Ridolfi, F. Zwirner, Phys. Lett. B **257**, 83 (1991)
5. J.R. Ellis, G. Ridolfi, F. Zwirner, Phys. Lett. B **262**, 477 (1991)
6. Y. Okada, M. Yamaguchi, T. Yanagida, Phys. Lett. B **262**, 54 (1991)
7. Y. Okada, M. Yamaguchi, T. Yanagida, Prog. Theor. Phys. **85**, 1 (1991)
8. A. Yamada, Phys. Lett. B **263**, 233 (1991)
9. H.E. Haber, R. Hempfling, Phys. Rev. Lett. **66**, 1815 (1991)
10. M. Drees, M.M. Nojiri, Phys. Rev. D **45**, 2482 (1992)
11. P.H. Chankowski, S. Pokorski, J. Rosiek, Phys. Lett. B **274**, 191 (1992)
12. P.H. Chankowski, S. Pokorski, J. Rosiek, Phys. Lett. B **286**, 307 (1992)
13. G. Degrassi, S. Heinemeyer, W. Hollik, P. Slavich, G. Weiglein, Eur. Phys. J. C **28**, 133 (2003). arXiv:hep-ph/0212020
14. S. Heinemeyer, W. Hollik, G. Weiglein, Eur. Phys. J. C **9**, 343 (1999). arXiv:hep-ph/9812472
15. S. Heinemeyer, W. Hollik, G. Weiglein, Comput. Phys. Commun. **124**, 76 (2000). arXiv:hep-ph/9812320
16. M. Frank et al., J. High Energy Phys. **0702**, 047 (2007). arXiv:hep-ph/0611326
17. M. Frank et al., http://www.feynhiggs.de
18. M. Carena, P. Draper, S. Heinemeyer, T. Liu, C.E.M. Wagner, G. Weiglein, Phys. Rev. D **83**, 055007 (2011). arXiv:1011.5304 [hep-ph]
19. O. Buchmueller et al., Phys. Lett. B **657**, 87 (2007). arXiv:0707.3447 [hep-ph]
20. O. Buchmueller et al., J. High Energy Phys. **0809**, 117 (2008). arXiv:0808.4128 [hep-ph]
21. O. Buchmueller et al., Eur. Phys. J. C **64**, 391 (2009). arXiv:0907.5568 [hep-ph]

22. O. Buchmueller et al., Phys. Rev. D **81**, 035009 (2010). arXiv:0912.1036 [hep-ph]
23. O. Buchmueller et al., Eur. Phys. J. C **71**, 1583 (2011). arXiv:1011.6118 [hep-ph]
24. O. Buchmueller et al., Eur. Phys. J. C **71**, 1634 (2011). arXiv:1102.4585 [hep-ph]
25. O. Buchmueller et al., Eur. Phys. J. C **71**, 1722 (2011). arXiv:1106.2529 [hep-ph]
26. For more information and updates, please see http://cern.ch/mastercode/
27. E.A. Baltz and P. Gondolo, JHEP **0410** (2004) 052. arXiv:hep-ph/0407039
28. B.C. Allanach, C.G. Lester, Phys. Rev. D **73**, 015013 (2006). arXiv:hep-ph/0507283
29. R.R. de Austri, R. Trotta, L. Roszkowski, J. High Energy Phys. **0605**, 002 (2006). arXiv:hep-ph/0602028
30. R. Lafaye, T. Plehn, M. Rauch, D. Zerwas, Eur. Phys. J. C **54**, 617 (2008). arXiv:0709.3985 [hep-ph]
31. S. Heinemeyer, X. Miao, S. Su, G. Weiglein, J. High Energy Phys. **0808**, 087 (2008). arXiv:0805.2359 [hep-ph]
32. R. Trotta, F. Feroz, M.P. Hobson, L. Roszkowski, R. Ruiz de Austri, J. High Energy Phys. **0812**, 024 (2008). arXiv:0809.3792 [hep-ph]
33. P. Bechtle, K. Desch, M. Uhlenbrock, P. Wienemann, Eur. Phys. J. C **66**, 215 (2010). arXiv:0907.2589 [hep-ph]
34. D. Feldman, K. Freese, P. Nath, B.D. Nelson, G. Peim, Phys. Rev. D **84**, 015007 (2011). arXiv:1102.2548 [hep-ph]
35. B.C. Allanach, Phys. Rev. D **83**, 095019 (2011). arXiv:1102.3149 [hep-ph]
36. S. Scopel, S. Choi, N. Fornengo, A. Bottino, Phys. Rev. D **83**, 095016 (2011). arXiv:1102.4033 [hep-ph]
37. P. Bechtle et al., Phys. Rev. D **84**, 011701 (2011). arXiv:1102.4693 [hep-ph]
38. B.C. Allanach, T.J. Khoo, C.G. Lester, S.L. Williams, J. High Energy Phys. **1106**, 035 (2011). arXiv:1103.0969 [hep-ph]
39. S. Akula, N. Chen, D. Feldman, M. Liu, Z. Liu, P. Nath, G. Peim, Phys. Lett. B **699**, 377 (2011). arXiv:1103.1197 [hep-ph]
40. M.J. Dolan, D. Grellscheid, J. Jaeckel, V.V. Khoze, P. Richardson, J. High Energy Phys. **1106**, 095 (2011). arXiv:1104.0585 [hep-ph]
41. S. Akula, D. Feldman, Z. Liu, P. Nath, G. Peim, Mod. Phys. Lett. A **26**, 1521 (2011). arXiv:1103.5061 [hep-ph]
42. M. Farina, M. Kadastik, D. Pappadopulo, J. Pata, M. Raidal, A. Strumia, Nucl. Phys. B **853**, 607 (2011). arXiv:1104.3572 [hep-ph]
43. S. Profumo, Phys. Rev. D **84**, 015008 (2011). arXiv:1105.5162 [hep-ph]
44. T. Li, J.A. Maxin, D.V. Nanopoulos, J.W. Walker, arXiv:1106.1165 [hep-ph]
45. N. Bhattacharyya, A. Choudhury, A. Datta, Phys. Rev. D **84**, 095006 (2011). arXiv:1107.1997 [hep-ph]
46. A. Fowlie, A. Kalinowski, M. Kazana, L. Roszkowski, Y.L.S. Tsai, Phys. Rev. D **85**, 075012 (2012). arXiv:1111.6098 [hep-ph]
47. R. Barate et al. (ALEPH, DELPHI, L3, OPAL Collaborations and LEP Working Group for Higgs boson searches), Phys. Lett. B **565**, 61 (2003). arXiv:hep-ex/0306033
48. S. Schael et al. (ALEPH, DELPHI, L3, OPAL Collaborations and LEP Working Group for Higgs boson searches), Eur. Phys. J. C **47**, 547 (2006). arXiv:hep-ex/0602042
49. http://tevnphwg.fnal.gov/ and references therein
50. ATLAS Collaboration, https://atlas.web.cern.ch/Atlas/GROUPS/PHYSICS/CONFNOTES/ATLAS-CONF-2011-132/ATLAS-CONF-2011-132.pdf
51. CMS Collaboration, http://cdsweb.cern.ch/record/1378096/files/HIG-11-020-pas.pdf
52. CMS Collaboration, https://cdsweb.cern.ch/ecord/1399607/files/HIG-11-023-pas.pdf
53. ATLAS Collaboration, https://cdsweb.cern.ch/record/1399599?ln=enATLAS-CONF-2011-157
54. L. Rolandi, on behalf of ATLAS, CMS and the LHC Higgs Combination Group, http://indico.in2p3.fr/getFile.py/access?contribId=72&sessionId=19&resId=0&materialId=slides&confId=6004
55. F. Gianotti for the ATLAS Collaboration, G. Tonelli for the CMS Collaboration, http://indico.cern.ch/conferenceDisplay.py?confId=164890
56. J. Ellis, J.R. Espinosa, G.F. Giudice, A. Hoecker, A. Riotto, Phys. Lett. B **679**, 369 (2009) and references therein
57. J. Ellis, D.A. Ross, Phys. Lett. B **506**, 331 (2001)
58. M. Drees, M.M. Nojiri, Phys. Rev. D **47**, 376 (1993). arXiv:hep-ph/9207234
59. G.L. Kane, C.F. Kolda, L. Roszkowski, J.D. Wells, Phys. Rev. D **49**, 6173 (1994). arXiv:hep-ph/9312272
60. H. Baer, M. Brhlik, Phys. Rev. D **53**, 597 (1996). arXiv:hep-ph/9508321
61. H. Baer, M. Brhlik, Phys. Rev. D **57**, 567 (1998). arXiv:hep-ph/9706509
62. J.R. Ellis, T. Falk, K.A. Olive, M. Schmitt, Phys. Lett. B **388**, 97 (1996). arXiv:hep-ph/9607292
63. J.R. Ellis, T. Falk, K.A. Olive, M. Schmitt, Phys. Lett. B **413**, 355 (1997). arXiv:hep-ph/9705444
64. J.R. Ellis, T. Falk, G. Ganis, K.A. Olive, M. Schmitt, Phys. Rev. D **58**, 095002 (1998). arXiv:hep-ph/9801445
65. V.D. Barger, C. Kao, Phys. Rev. D **57**, 3131 (1998). arXiv:hep-ph/9704403
66. J.R. Ellis, T. Falk, G. Ganis, K.A. Olive, Phys. Rev. D **62**, 075010 (2000). arXiv:hep-ph/0004169
67. J.R. Ellis, T. Falk, G. Ganis, K.A. Olive, M. Srednicki, Phys. Lett. B **510**, 236 (2001). arXiv:hep-ph/0102098
68. V.D. Barger, C. Kao, Phys. Lett. B **518**, 117 (2001). arXiv:hep-ph/0106189
69. L. Roszkowski, R. Ruiz de Austri, T. Nihei, J. High Energy Phys. **0108**, 024 (2001). arXiv:hep-ph/0106334
70. A. Djouadi, M. Drees, J.L. Kneur, J. High Energy Phys. **0108**, 055 (2001). arXiv:hep-ph/0107316
71. U. Chattopadhyay, A. Corsetti, P. Nath, Phys. Rev. D **66**, 035003 (2002). arXiv:hep-ph/0201001
72. J.R. Ellis, K.A. Olive, Y. Santoso, New J. Phys. **4**, 32 (2002). arXiv:hep-ph/0202110
73. H. Baer, C. Balazs, A. Belyaev, J.K. Mizukoshi, X. Tata, Y. Wang, J. High Energy Phys. **0207**, 050 (2002). arXiv:hep-ph/0205325
74. R. Arnowitt, B. Dutta, arXiv:hep-ph/0211417
75. J.R. Ellis, K.A. Olive, Y. Santoso, V.C. Spanos, Phys. Lett. B **565**, 176 (2003). arXiv:hep-ph/0303043
76. H. Baer, C. Balazs, J. Cosmol. Astropart. Phys. **0305**, 006 (2003). arXiv:hep-ph/0303114
77. A.B. Lahanas, D.V. Nanopoulos, Phys. Lett. B **568**, 55 (2003). arXiv:hep-ph/0303130
78. U. Chattopadhyay, A. Corsetti, P. Nath, Phys. Rev. D **68**, 035005 (2003). arXiv:hep-ph/0303201
79. C. Munoz, Int. J. Mod. Phys. A **19**, 3093 (2004). arXiv:hep-ph/0309346
80. R. Arnowitt, B. Dutta, B. Hu, arXiv:hep-ph/0310103
81. J. Ellis, K.A. Olive, in *Particle Dark Matter*, ed. by G. Bertone (2010), pp. 142–163. arXiv:1001.3651 [astro-ph.CO]
82. J.R. Ellis, D.V. Nanopoulos, K.A. Olive, Y. Santoso, Phys. Lett. B **633**, 583 (2006). hep-ph/0509331
83. H. Baer, A. Mustafayev, S. Profumo, A. Belyaev, X. Tata, Phys. Rev. D **71**, 095008 (2005). arXiv:hep-ph/0412059
84. H. Baer, A. Mustafayev, S. Profumo, A. Belyaev, X. Tata, J. High Energy Phys. **0507**, 065 (2005). hep-ph/0504001

85. J.R. Ellis, K.A. Olive, P. Sandick, Phys. Rev. D **78**, 075012 (2008). arXiv:0805.2343 [hep-ph]
86. E. Aprile et al. (XENON100 Collaboration), Phys. Rev. Lett. **107**, 131302 (2011). arXiv:1104.2549 [astro-ph.CO]
87. S. Heinemeyer et al., J. High Energy Phys. **0608**, 052 (2006). arXiv:hep-ph/0604147
88. S. Heinemeyer, W. Hollik, A.M. Weber, G. Weiglein, J. High Energy Phys. **0804**, 039 (2008). arXiv:0710.2972 [hep-ph]
89. B.C. Allanach, Comput. Phys. Commun. **143**, 305 (2002). arXiv:hep-ph/0104145
90. G. Isidori, P. Paradisi, Phys. Lett. B **639**, 499 (2006). arXiv:hep-ph/0605012
91. G. Isidori, F. Mescia, P. Paradisi, D. Temes, Phys. Rev. D **75**, 115019 (2007). arXiv:hep-ph/0703035, and references therein
92. F. Mahmoudi, Comput. Phys. Commun. **178**, 745 (2008). arXiv:0710.2067 [hep-ph]
93. F. Mahmoudi, Comput. Phys. Commun. **180**, 1579 (2009). arXiv:0808.3144 [hep-ph]
94. D. Eriksson, F. Mahmoudi, O. Stal, J. High Energy Phys. **0811**, 035 (2008). arXiv:0808.3551 [hep-ph]
95. A. Arbey, F. Mahmoudi, Comput. Phys. Commun. **181**, 1277 (2010). arXiv:0906.0369 [hep-ph]
96. G. Belanger, F. Boudjema, A. Pukhov, A. Semenov, Comput. Phys. Commun. **176**, 367 (2007). arXiv:hep-ph/0607059
97. G. Belanger, F. Boudjema, A. Pukhov, A. Semenov, Comput. Phys. Commun. **149**, 103 (2002). arXiv:hep-ph/0112278
98. G. Belanger, F. Boudjema, A. Pukhov, A. Semenov, Comput. Phys. Commun. **174**, 577 (2006). arXiv:hep-ph/0405253
99. Information about this code is available from K.A. Olive: it contains important contributions from T. Falk, A. Ferstl, G. Ganis, A. Mustafayev, J. McDonald, K.A. Olive, P. Sandick, Y. Santoso and M. Srednicki
100. P. Skands et al., J. High Energy Phys. **0407**, 036 (2004). arXiv:hep-ph/0311123
101. B. Allanach et al., Comput. Phys. Commun. **180**, 8 (2009). arXiv:0801.0045 [hep-ph]
102. G. Aad et al. (ATLAS Collaboration), Phys. Lett. B **710**, 67 (2012). arXiv:1109.6572 [hep-ex]
103. S. Chatrchyan et al. (CMS Collaboration), Phys. Rev. Lett. **107**, 221804 (2011). arXiv:1109.2352 [hep-ex]
104. S. Chatrchyan et al. (CMS Collaboration), Phys. Rev. Lett. **107**, 191802 (2011). arXiv:1107.5834 [hep-ex]
105. R. Aaij et al. (LHCb Collaboration), Phys. Lett. B **699**, 330 (2011). arXiv:1103.2465 [hep-ex]
106. R. Aaij et al. (LHCb Collaboration), Phys. Lett. B **708**, 55 (2012). arXiv:1112.1600 [hep-ex]
107. T. Aaltonen et al. (CDF Collaboration), Phys. Rev. Lett. **107**, 239903 (2011)
108. T. Aaltonen et al. (CDF Collaboration), Phys. Rev. Lett. **107**, 191801 (2011). arXiv:1107.2304 [hep-ex]
109. S.S. AbdusSalam et al., Eur. Phys. J. C **71**, 1835 (2011). arXiv:1109.3859 [hep-ph]
110. P. Gondolo, J. Edsjo, P. Ullio, L. Bergstrom, M. Schelke, E.A. Baltz, J. Cosmol. Astropart. Phys. **0407**, 008 (2004). arXiv:astro-ph/0406204
111. http://www.physto.se/~edsjo/darksusy/